Vapor−Liquid Phase Coexistence, Critical Properties, and Surface Tension of Confined Alkanes

Sudhir K. Singh, Ankit Sinha, Goutam Deo, and Jayant K. Singh*

Department of Chemical Engineering, Indian Institute of Technology Kanpur, Kanpur 208016, India

Received: August 18, 2008; Revised Manuscript Received: March 17, 2009

Configurational-bias grand-canonical transition-matrix Monte Carlo simulations are conducted to investigate various thermophysical properties, such as phase coexistence, critical properties, density and orientation profiles of liquid and vapor phases, and vapor−liquid surface tension of methane, ethane, propane, *n*-butane, and *n*-octane in bulk and slit pores of graphite and mica surfaces. An exponential-6 (exp-6) model is used for the investigation of normal alkanes with a cutoff radius, 15 Å. It is found that the surface tension of the bulk *n*-alkane, C_1-C_4, based on a truncated exp-6 model, agrees reasonably well with the experimental data. Critical properties are reported by means of the rectilinear diameter approach and least-squares technique. The shift in the critical temperature under confinements follows more than two linear regimes with an inverse in the slit width, as the slit width approaches the two-dimensional limit. This is contrary to what has been previously reported in the literature. The behavior of the critical temperature shift is sensitive to the nature of the surface. The critical density, on the other hand, fluctuates with a decrease in the slit width. The shift in the critical vapor pressure continuously increases with a decrease in the slit width toward the two-dimensional value and becomes constant for pore sizes less than 5 Å for the fluid studied in this work. Corresponding state plots suggest that the deviation of the saturation vapor pressure from the bulk saturation pressure under confinement is positive for large pores and negative for smaller pores. Vapor−liquid surface tension values for *n*-alkanes, in both types of slit pores, are computed via the finite-size scaling method of Binder and compared with their bulk values. Our investigation reveals that under slit-pore confinement the vapor−liquid surface tension decreases many fold.

1. Introduction

Alkanes are commonly used in various industries. They are present in lubricants, fuels, polymers, surfactants, and liquid crystals as well as many biological molecules such as lipids. Understanding the behavior of alkanes under nanoconfinements is of great interest from fundamental and practical perspectives. In general, fluids under any type of confinement within pores of nanometer size exhibit significant deviation from bulk thermophysical and structural properties.[1] Such systems are in between bulk matter and single atoms or molecules, and as a consequence, finite-size and surface effects become imperative for the investigation of such systems. Any real system interfaces either with walls of a container or with different phases of the substance under consideration. An extra free energy contribution arises because of these interfaces, which plays an important role in nanoconfined systems and affects the state of the substance. Interplay of fluid−wall and fluid−fluid forces can lead to fascinating surface-driven phase changes and various other thermophysical and interfacial phenomena. The fundamental interest in these phase changes and other related properties is to understand the new physics that results from finite-size effects, varying dimensionality, and surface forces. In addition, a fundamental understanding of the various thermophysical and interfacial phenomena, in the presence of surfaces, is necessary for many industrial and geophysical operations. For example, micro- and mesoporous materials are widely used in chemical, oil and gas, food, and pharmaceutical industries for pollution control, mixture separation, and purification and as catalysts and catalyst supports for chemical reactions.[2−13] The design of such processes is largely empirical with an underdeveloped scientific basis because the theory-based understanding of confined fluids is still not completely understood.[14−18] However, with a rapid increase of computer power and advanced algorithms, molecular simulation can help to understand the underlying physics of confinement effects on various thermophysical and interfacial properties, which could lead to significant improvements in these industrial processes.

Molecular simulations have been used to study the adsorption properties and isotherms of single-component and binary mixtures of normal and branched alkanes in various porous materials such as zeolites.[19−23] Capillary phase transitions and adsorption and separation properties of mixtures of *n*-alkanes in a carbon nanotube were studied using gauge-cell Monte Carlo simulation.[24,25] It was observed by the investigators that confinement of *n*-alkanes in a carbon nanotube decreases its critical temperature and increases its critical density. Recently, molecular simulation has been applied as a screening tool to identify the new materials for adsorption applications. Such an approach was used for metal−organic frameworks[26,27] to study the adsorption characteristics of novel metal−organic materials for methane and hydrogen storage applications. Zhang[28] used a molecular dynamics simulation technique to study the density profiles, structural properties, and average diffusion coefficients of *n*-decane in a carbon nanotube. The author observed well-defined peaks in the density profiles, which indicated a strong tendency of layer formation in the nanotube. Further, the structural properties were found to vary strongly with the radial position of the chain's center of mass. In some recent work,

* Corresponding author. E-mail: jayantks@iitk.ac.in.

10.1021/jp8073915 CCC: $40.75
Published on Web 04/07/2009

single-component adsorption of methane, [29,30] ethane,[31−33] and some other higher *n*-alkanes[34,35] along with its adsorption isotherms and density and orientation profiles was investigated in carbon slit pores using Monte Carlo simulations. Furthermore, there have been numerous molecular dynamics simulations for chain molecules in slit pores. These molecular dynamics simulations were used to examine the density profiles and chain conformations of linear and branched alkanes under shear-flow conditions.[4,36−40] These investigations indicate that there is a profound influence of the slit surfaces on the fluid structure. However, in all of the above-mentioned work, authors did not investigate rigorously changes in the critical and vapor−liquid interfacial properties under confinement with changes in the pore width, particularly those approaching the two-dimensional limit. This is the major objective of the current work. In this work, we have investigated thermophysical properties of *n*-alkanes confined in graphite and mica slit pores. In particular, we present the phase coexistence properties (saturated densities and vapor pressures), critical properties (critical temperature, pressure, and density), local density and orientation profiles of liquid and vapor phases, and interfacial properties (vapor−liquid surface tension) of *n*-alkanes of chain length $C_1-C_{8,}$ with changes in the slit-width, temperature, and surface characteristics. The paper is organized as follows. Section 2 outlines the potential models and simulation details. In section 3, we present the results of our investigation, and we conclude in section 4.

2. Simulation Methods

2.1. Potential Model. A united-atom approach[41] is used to model the *n*-alkane molecules. Nonbonded site−site interactions are described with the modified Buckingham exponential intermolecular potential of Errington and Panagiotopoulos,[42] for which the pair interaction energy, U, is represented as

$$U(r) = \left\{ \frac{\varepsilon}{1-\frac{6}{\alpha}} \left[\frac{6}{\alpha} \exp\left(\alpha \left[1 - \frac{r}{r_m} \right] \right) - \left(\frac{r_m}{r} \right)^6 \right] \right\} \quad \text{for } r > r_{max}$$

$$= \infty \quad \text{for } r < r_{max} \tag{1}$$

where ε, r_m, and α are adjustable parameters. The variable r_m is the radial distance at which $U(r)$ reaches a minimum, and the cutoff distance r_{max} represents the smallest radial distance for which $d[U(r)]/d(r) = 0$. The radial distance for which $U(r) = 0$ is denoted by σ. The parameters ε, σ, and α are 129.63 K, 3.679 Å, and 16, respectively, for the methyl group ($-CH_3$), 73.5 K, 4.00 Å, and 22, respectively, for the methylene group ($-CH_2-$), and 160.3 K, 3.73 Å, and 15, respectively, for CH_4. The following combining rules are used to determine the cross parameters:

$$\sigma_{ij} = \frac{1}{2}(\sigma_i + \sigma_j)$$

$$\varepsilon_{ij} = (\varepsilon_i \varepsilon_j)^{1/2}$$

$$\alpha_{ij} = (\alpha_i \alpha_j)^{1/2} \tag{2}$$

The bond lengths CH_3-CH_3, CH_3-CH_2, and CH_2-CH_2 are 1.839, 1.687, and 1.535 Å, respectively. Bond-bending angles are generated according to the bending potential[43]

$$u_{bend}(\theta) = \frac{K_\theta}{2}(\theta - \theta_{eq})^2 \tag{3}$$

where $K_\theta = 62\,500$ K/rad^2 and $\theta_{eq} = 114°$. Torsion angles are generated according to the potential[44]

$$u_{tor}(\varphi) = V_0 + \frac{V_1}{2}(1 + \cos\varphi) + \frac{V_2}{2}(1 - \cos 2\varphi) + \frac{V_3}{2}(1 + \cos 3\varphi) \tag{4}$$

where $V_0 = 0$, $V_1 = 355.03$ K, $V_2 = -68.19$ K, and $V_3 = 791.32$ K.

In this work, pore is of slit geometry with smooth and structureless surfaces. Wall−fluid interaction is described by the 9−3 Steele potential:[45]

$$\varphi_{wf}(z) = \frac{2}{3}\pi\rho_w\varepsilon_{wf}\sigma_{wf}^3\left\{ \frac{2}{15}\left(\frac{\sigma_{wf}}{z}\right)^9 - \left(\frac{\sigma_{wf}}{z}\right)^3 \right\} \tag{5}$$

where$Z$ is the distance of the fluid particle from the wall and ρ_w, ε_{wf}, and σ_{wf} are the parameters of the Steele potential. In eq 5, $\sigma_{wf} = (\sigma_w + \sigma_{ii})/2$ where σ_w denotes the "diameter" of a wall atom and σ_{ii} refers to the molecular diameter of corresponding CH_2-CH_2 or CH_3-CH_3- interactions. Potential parameters, ρ_w, ε_{wf}, and σ_w for graphite and mica surfaces are 0.033 Å^{-3}, 84 K, and 3.92 Å and 0.097 Å^{-3}, 100 K, and 2.22 Å, respectively, whereas for methane σ_{wf} for graphite and mica surfaces are 3.7995 and 2.9805 Å, respectively.[46]

2.2. Simulation Details. In this work, we have used a configurational-bias[47−49] grand-canonical transition-matrix Monte Carlo (GC-TMMC)[50,51] simulation scheme to explore the configuration space more efficiently. A configurational-bias Monte Carlo technique is incorporated within the GC-TMMC framework along with a multicanonical sampling scheme.[52] In this approach, Monte Carlo simulations are conducted in a standard grand-canonical ensemble, where the volume (V), chemical potential (μ), and temperature (T) are held constant and the particle number (N, density) and energy (U) fluctuates. During a simulation, attempted transitions between states of different densities are monitored.[53,54] At regular intervals during a simulation, this information is used to obtain an estimate of the density probability distribution, which is subsequently used to bias the sampling to low probability densities. Over time, all densities of interest are sampled adequately. The result is an efficient self-adaptive method for determining the density probability distribution over a specified range of densities (typically a range that corresponds to the densities of two potentially coexisting phases). Once a probability distribution has been collected at a given value of the chemical potential (μ_0), histogram reweighting[55] is used to shift the probability distribution to other values of the chemical potential using the following relationship:

$$\ln \Pi(N,\mu) = \ln \Pi(N,\mu_0) + \beta(\mu - \mu_0)N \tag{6}$$

To determine the coexistence chemical potential, we apply the above relationship to estimate the chemical potential that produces a coexistence probability distribution. Saturated densities are related to the first moment of the vapor and liquid peaks of the coexistence probability distribution, $\Pi_c(N)$. To calculate the saturation pressure, we use the following expression:

$$\beta PV = \ln[\sum \Pi_c(N)/\Pi_c(0)] - \ln(2) \tag{7}$$

In addition to the calculation of the saturation pressure, densities, and energies, GC-TMMC simulation can also yield the interfacial free energy, βF_L, for a finite system size with a cell length L, which is determined from the maximum likelihood in the liquid (Π^l_{max}) and vapor (Π^v_{max}) regions and the minimum likelihood in the interface region (Π_{min}):

$$\beta F_L = \frac{1}{2}(\ln \Pi^l_{max} + \ln \Pi^v_{max}) - \ln \Pi_{min} \tag{8}$$

This method does not require the establishment and maintainance of an interface, as is necessary in slab-based methods.[56]

From the formalism of Binder,[57] the infinite-size interfacial free energy of a two-dimensional surface can be evaluated using the following relationship:

$$\beta\gamma_L = \frac{\beta F_L}{2S} = C_1\frac{1}{S} + C_2\frac{\ln L}{S} + \beta\gamma_\infty \quad (9)$$

where γ_L is the apparent system size-dependent surface tension and γ_∞ is the infinite-system size ($L \rightarrow \infty$) surface tension, S is the interface area (LH), L and H are the simulation cell size and pore width, respectively, and C_1 and C_2 are constants. The expression (9) suggests that the group $\beta F_L/2S$ becomes linear with the scaling variable $(\ln L)/S$ as the system size approaches infinity. The method enables one to evaluate the infinite-system size interfacial tension by extrapolating a series of finite-system size interfacial free energies. This approach has now been applied to obtain the surface tension of various fluids[58−61] but mainly in the bulk phase. Recently, we have applied it for the evaluation of the vapor−liquid surface tension of a confined square-well fluid.[62]

In this work, we have estimated the vapor−liquid critical parameter by fitting the coexistence densities to the law of the rectilinear diameter[63] and the scaling law for the density.[64]

$$\rho_l - \rho_v = B\left(1 - \frac{T}{T_c}\right)^\beta \quad (10)$$

$$(\rho_l + \rho_v)/2 = \rho_c + A\left(1 - \frac{T}{T_c}\right) \quad (11)$$

where ρ_l, ρ_v, ρ_c, T_c, and β are the liquid-phase density, vapor-phase density, critical density, critical temperature, and critical exponent, respectively.

The critical pressure, P_c, is calculated using the least-squares fitting of the saturation pressure data obtained from the GC-TMMC simulations to the following expression, which has a form similar to that of the Antoine equation:

$$\ln P_c = A - \frac{B}{T_c} \quad (12)$$

where A and B are adjustable parameters. The above empirical form is also utilized to obtain the critical pressure for confined fluids, as shown earlier for a confined square-well fluid.[62]

The saturated z density profiles (profiles perpendicular to the slit surface), ρ_z, are obtained by recording $\rho(N,z)$ for each particle number sampled during GC-TMMC simulations. Coexistence density profiles are finally obtained using the following expression:

$$\rho(z)_{\text{vapor/liquid}} = \frac{\sum_{i\in \text{vapor/liquid}} \Pi_c(i)\,\rho(i,z)}{\sum_{i\in \text{vapor/liquid}} \Pi_c(i)} \quad (13)$$

where i is the particle number and its range varies for liquid and vapor phases.

The orientation of the molecules in the slit pore is evaluated using the following orientation order parameter (S_z), which is defined as

$$S_z = \left\langle \frac{3\cos\alpha - 1}{2} \right\rangle \quad (14)$$

where α is defined as the angle between the head-to-tail vector of the alkane molecule and the z axis. S_z is evaluated for coexistence liquid and vapor phases akin to the calculation of coexistence density profiles, as described above. The orientation order parameter takes a value of 1 if all of the molecules are aligned perpendicularly to the wall, a value of −0.5 if they are all parallel to the walls, and a value of 0 if they are randomly oriented.

To perform the simulations in an efficient manner, we take advantage of the fact that the TMMC algorithm enables one to fill the overall collection matrix through a series of independent simulations, each restricted to a limited range of macrostates. In this work, we used a scheme in which a series of semi-independent simultaneous simulations sample overlapping windows in the macrostates with periodic swapping of configurations between processors. Further details can be found in ref 65. In our simulations, the Monte Carlo move distribution for

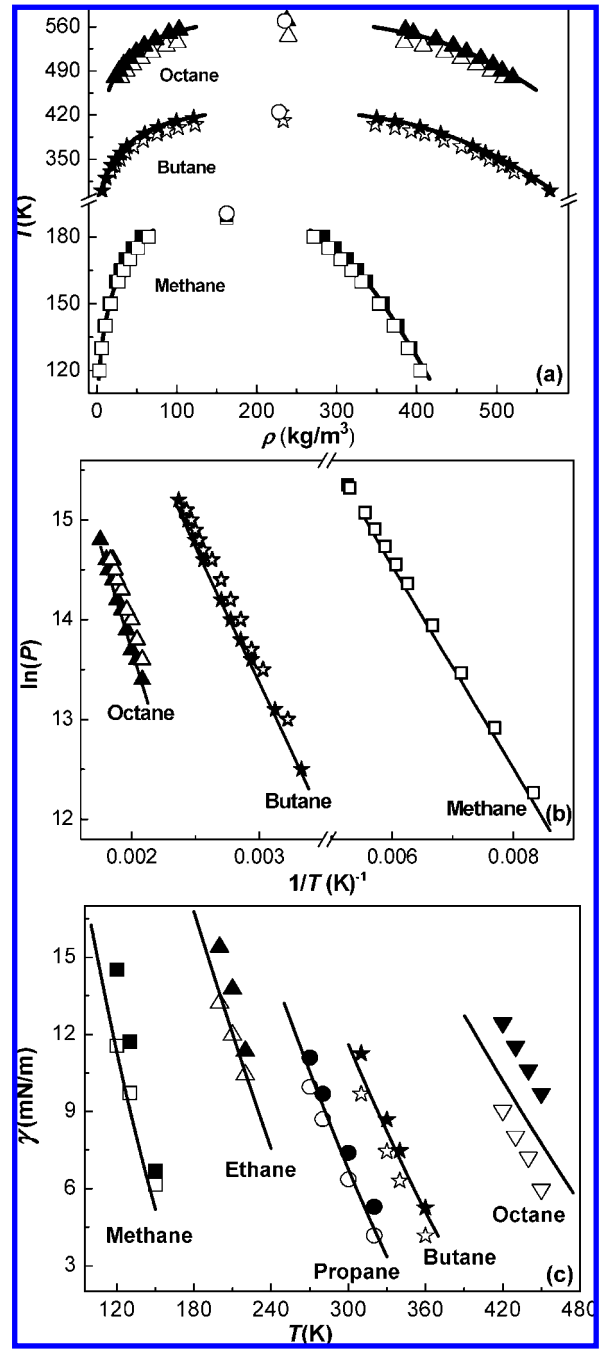

Figure 1. (a) Vapor−liquid coexistence envelope, (b) saturation pressure, and (c) vapor−liquid surface tension of bulk methane, *n*-butane, and *n*-octane. Solid lines and filled and open symbols represent the data of the experiments,[68] the exp-6 model with full range interaction, and the exp-6 model with r_c = 15 Å, respectively. The error bars are smaller than the symbol size.

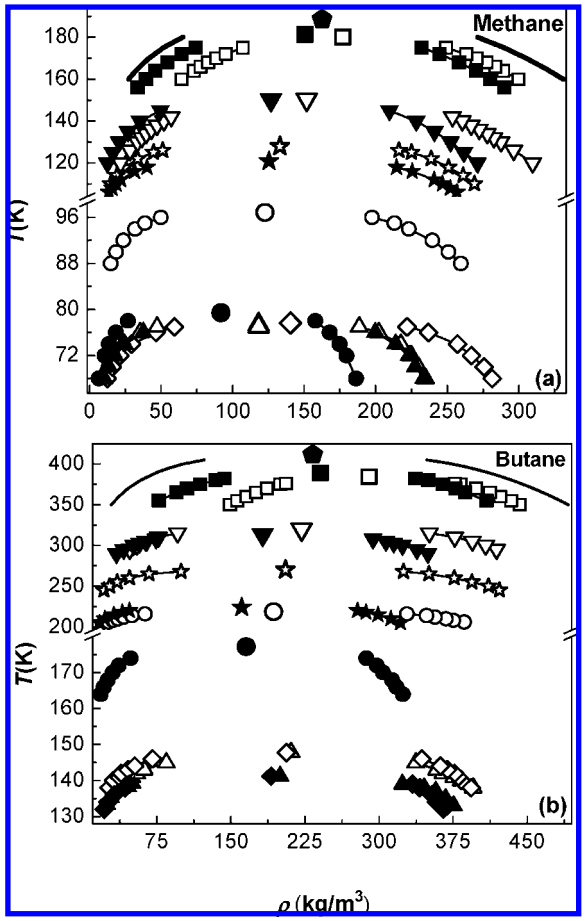

Figure 2. Vapor−liquid coexistence envelopes of alkanes in graphite and mica slit pores: (a) methane; (b) *n*-butane. Solid curves represent bulk simulation data with pentagons as the bulk critical points. Filled symbols represent graphite (G) slit pores and open symbols mica (M) slit pores. In part a, symbols square, inverted-triangle, star, circle, triangle, and diamond represent slit widths of 40, 15, 10, 8, 6, and 5 Å, respectively. In part b, filled diamond and triangle symbols represent 6 and 5.8 Å, respectively, and open diamond and triangle symbols represent 5.7 and 5.5 Å slit widths, respectively; other symbols have the same meanings as those in part a. The error bars are smaller than the symbol size.

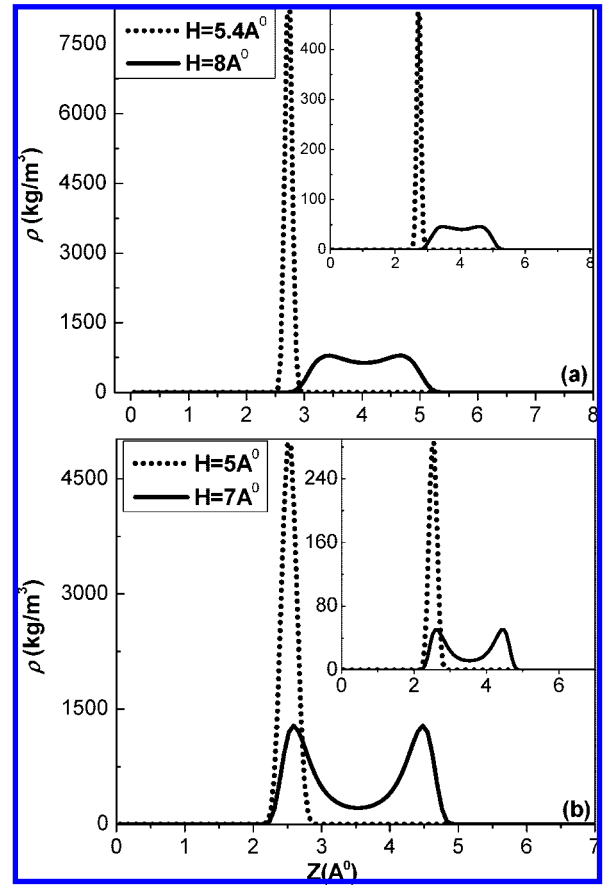

Figure 3. Local *z*-density profiles of the saturated vapor phase, in the inset, and the saturated liquid phase of methane in (a) graphite and (b) mica slit pores, respectively, at a reduced temperature, $T_R = 0.90$.

evaluating phase coexistence properties is as follows: 15% particle displacement, 50% particle insertion/deletion, 15% particle rotation, and 20% particle regrowth. In the finite-size scaling approach, the maximum number of particles taken in this work varied from around 2100 particles for methane to 1400 particles for octane. The simulations are performed with truncated nonbonded interaction without long-range correction (LRC) unless otherwise stated. Three independent runs are conducted to obtain the statistical error in the coexistence density, pressure, and vapor−liquid surface tension. The errors in the coexistence density, vapor pressure, and surface tension of bulk *n*-alkanes are less than 1%, 0.4%, and 4%, respectively. On the other hand, statistical errors in the saturated density, pressure, and vapor−liquid surface tension of confined *n*-alkanes are less than 3%, 1.5%, and 5%, respectively. Errors in T_c, ρ_c, and P_c of bulk *n*-alkanes are less than 0.3%, 0.7%, and 3.5%, respectively, whereas errors in T_c, ρ_c, and P_c of confined *n*-alkanes are less than 0.4%, 1.5%, and 4.2%, respectively.

3. Results and Discussion

It has been observed that the cutoff radius of the intermolecular potential influences the phase equilibrium and interfacial properties.[66] Earlier, Goujon and co-workers[67] have investigated the effect of the cutoff radius, r_c, on the liquid−vapor surface tension of *n*-pentane using the TraPPE model. The authors found the TraPPE model with $r_c = 17$ Å, a reasonably good model for the prediction of the bulk coexistence density and surface tension of *n*-pentane. In our earlier work, some of us compared the bulk and interfacial properties of the exp-6 model of normal butane, hexane, and octane with the experimental values. The exp-6 model though predicts the bulk coexistence property exceedingly well; however, it overpredicts the surface tension by 26%. In this work, we first investigate the effect of the cutoff radius with $r_c = 15$ Å on the bulk and interfacial properties of the exp-6 model and compare it with the literature values. The results for the surface tension of bulk methane, ethane, and propane using the full exp-6 model (nontruncated form) are new and were not reported earlier. Figure 1a shows the bulk phase coexistence curve of C_1, C_4, and C_8 based on the truncated exp-6 model with $r_c = 15$ Å and the full exp-6 model along with experimental data.[68] It is known that the full exp-6 model predicts the phase equilibrium data of *n*-alkane accurately, which also is reflected from Figure 1. Phase coexistence data calculated with $r_c = 15$ Å without LRC, for methane, also appear to be in good agreement with the experimental data. However, for the case of butane and octane, saturated vapor densities are overestimated whereas saturated liquid densities are underestimated slightly with the implementation of the cutoff radius, $r_c = 15$ Å without LRC. Because of the shrinkage of the coexistence envelope, the critical temperature is underestimated by 3−4% for butane and *n*-octane, respectively, whereas the critical density is overestimated by 2% for both fluids. Figure

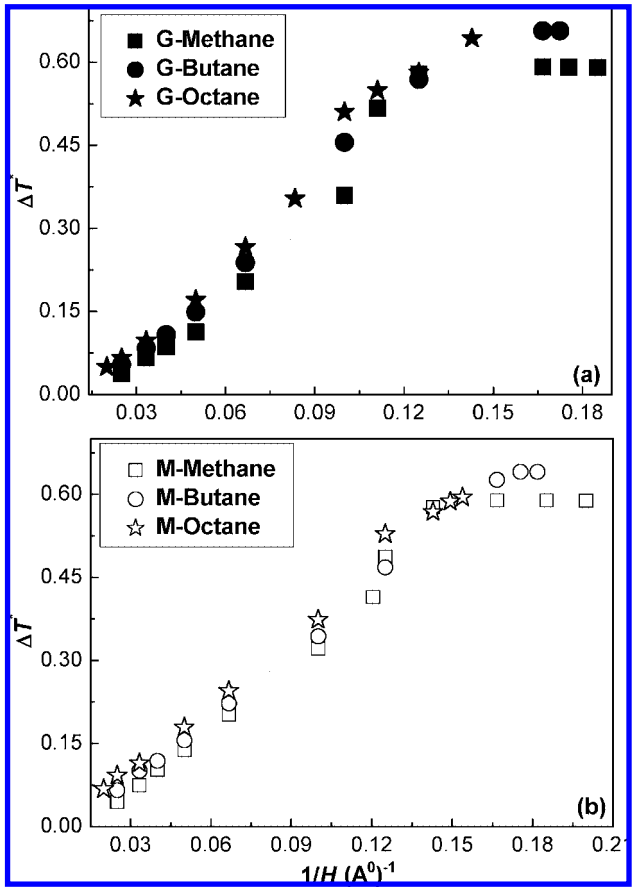

Figure 4. Shift in the critical temperature ΔT^* vs inverse of the slit width (H) for n-alkanes in (a) graphite and (b) mica slit pores.

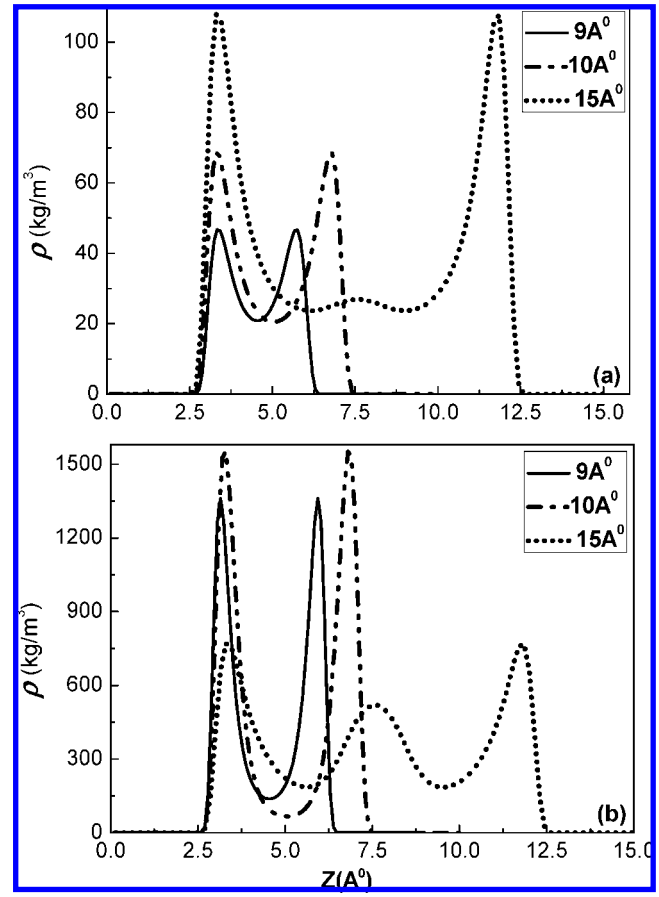

Figure 5. Local z-density profiles of (a) the saturated vapor phase and (b) the saturated liquid phase of methane in graphite slit pores of three different slit widths at a reduced temperature, $T_R = 0.90$.

1b presents the saturation vapor pressure of the bulk n-alkanes. The behavior of the vapor pressure for the truncated exp-6 model is similar to that seen for the orthobaric densities. The critical pressure for the truncated exp-6 model, with $r_c = 15$ Å, is underestimated by 1.8%, 7.6%, and 8.6% for methane, butane, and n-octane, respectively. On the other hand, the full exp-6 model (nontruncated form) overestimates the critical pressure by 1.25%, 6.3%, and 6.5% for methane, butane, and n-octane, respectively.

The vapor−liquid surface tension is evaluated using a finite-size scaling approach in a way similar to that reported in our earlier work.[69] The surface tension based on n-alkane with the truncated exp-6 model, with $r_c = 15$ Å, is in good agreement with the experimental data for methane and ethane; however, for the larger alkanes, the truncated potential underestimates the surface tension, as shown in Figure 1c. The deviation from the experimental data gradually increases from propane to octane. Our current investigation along with earlier work[69] shows that the exp-6 model with full range interaction overestimates the surface tension value of C_1-C_8 by 26%. On the other hand, with a fixed $r_c = 15$ Å without LRC, the average absolute deviation from the experimental values for methane, ethane, propane, butane, and octane are 9, 2, 5, 12, and 16%, respectively. To study the various coexistence and interfacial properties under different slit-pore confinements, we have used a cutoff radius $r_c = 15$ Å without LRC in this work. This choice of the cutoff radius seems to be reasonable based on the analysis that most properties deviate slightly from the experimental values for C_1-C_8.

Phase coexistence properties and critical properties of n-alkanes of carbon chains C_1, C_4, and C_8 are investigated in graphite and mica slit pores of various slit widths. Typical phase coexistence envelopes of methane and butane are shown in parts a and b of Figure 2, respectively, which present the transformation of the behavior from nearly three-dimensionally to two-dimensionally induced by the confinement. A large fraction of the confined molecules experience a reduction in the number of nearest-neighbor molecules; hence, under confinement, a lowering of the critical temperature is observed. The critical temperature continues to decrease with a decrease in the slit width up to a certain extent, which for all of the cases is close to two to three molecular diameters. A subsequent decrease in the slit width has no effect on the critical temperature, and it appears to become constant. The critical density, on the contrary, oscillates as we approach from bulk to two-dimensional geometry, as observed in Figure 2a,b. In general, the critical density at a large pore is higher than the bulk critical density. This is due to the layering of molecules in the vapor phase near the surface, which increases the density of the vapor phase. The stronger the surface, the higher would be the vapor density, leading to higher critical density. However, such behavior is absent in smaller pores because of the decrease in saturated liquid densities. This trend is observed for all of the studied cases of alkanes, C_1, C_4, and C_8, except for methane in a graphite slit pore, which has shown lower critical density even for higher slit width, which is probably due to the relatively less effect of the graphite surface on the vapor-phase density. Recently, Jiang and Sandler observed similar behavior of higher critical density and a lowering of the critical temperature for C_1-C_8 in a carbon nanotube.[25] In addition, we observed that, as the system approaches the two-dimensional regime, the critical density

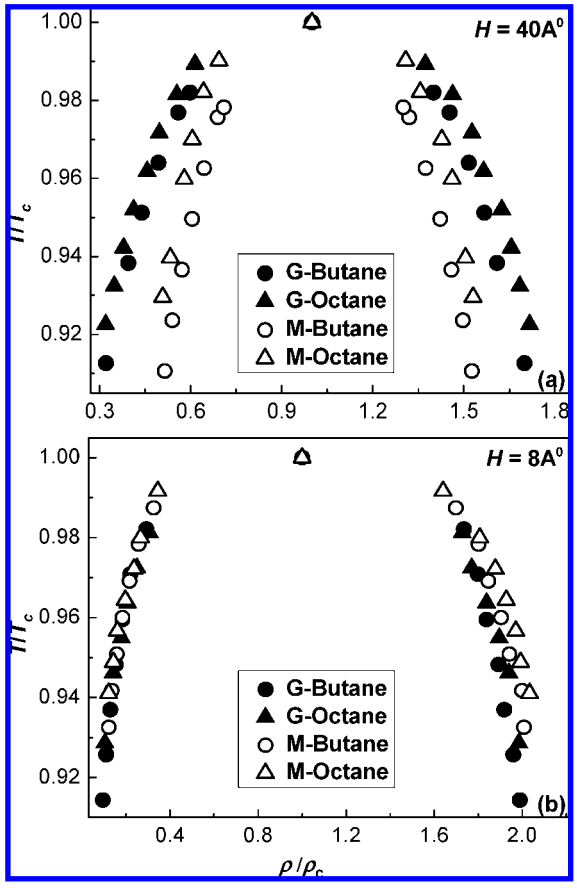

Figure 6. Corresponding state plot of vapor−liquid coexistence envelopes of *n*-butane and *n*-octane in graphite (G) and mica (M) pores for two different slit widths.

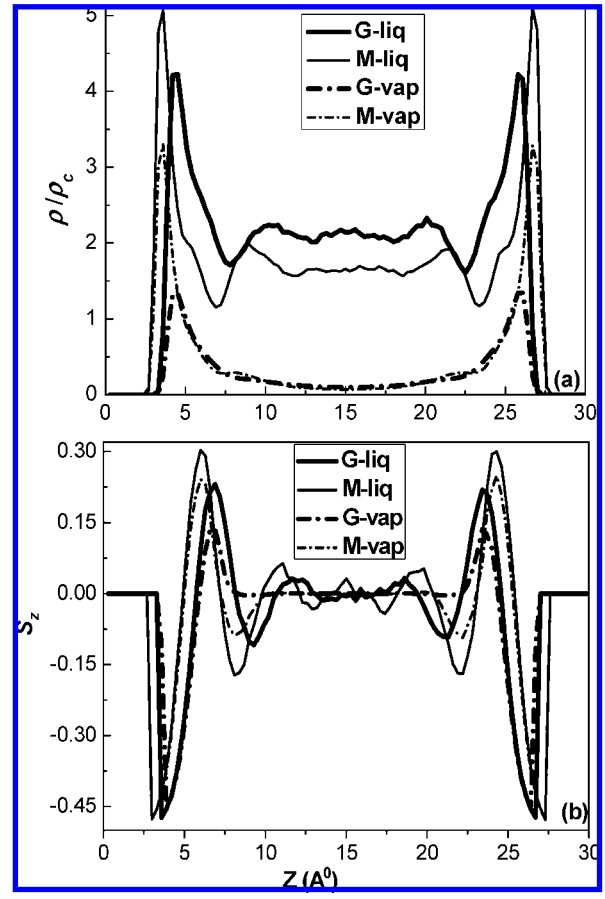

Figure 7. (a) Reduced local *z*-density and (b) orientation profiles of saturated vapor and liquid phases of *n*-octane in graphite (G) and mica (M) slit pores at a fixed slit width, 30 Å, and at a reduced temperature, $T_R = 0.93$.

increases toward the two-dimensional value even though the critical temperature is almost constant. To understand this behavior, we studied the coexistence vapor and liquid density profiles at extremely small pores. Parts a and b of Figure 3 present the *z*-density profiles of methane at a reduced temperature $T_R = T/T_c = 0.90$ in graphite and mica slit pores, respectively, at two different slit widths. Figure 3a depicts that in a graphite slit pore of slit width 5.4 Å, coexistence vapor and liquid densities are more than that in a 8 Å slit pore; however, the relative increase in the liquid-phase density is larger than that in the vapor-phase density as the slit width is reduced from 8 to 5.4 Å. This is also visible in the coexistence envelope of methane in Figure 2a. This clearly explains the increase in the critical density even though the critical temperature remains insensitive to the decrease in the slit pore with a slit width of less than 8 Å. Similar behaviors of methane in mica slit pores with slit widths of 5 and 7 Å are observed, as seen in Figure 3b.

Bruno et al.[70] and Vishnyakov et al.[71] reported that the shift in the critical temperature, $\Delta T^* = (T_{cb} - T_{cp})/T_{cb}$, where T_{cb} is the critical temperature of the bulk fluid and T_{cp} is the critical temperature of the confined fluid, for small pores, is roughly inversely proportional to the slit width. Parts a and b of Figure 4 present the shift in the critical temperature against the inverse of the slit width for the two different types of slit pore confinements, graphite (G) and mica (M), which depict more than two linear regimes for the critical temperature. Our observations are in good agreement with the investigation of Bruno et al. and Vishnyakov et al. but for pore sizes larger than approximately three molecular diameters is not extensible for smaller pore size. The slope of the critical temperature shift against the inverse of the slit width is observed to change at smaller pore size and, in particular, first increases for the studied system and subsequently approaches zero near the two-dimensional limit. For example, in the case of a graphite−methane system, as shown in Figure 4a, the rate of the critical temperature shift is found to increase with a decrease in the slit width from 10 to 9 Å, which is relatively higher compared to that seen for a pore size higher than 10 Å. This interesting behavior is due to changes in the coexisting liquid and vapor densities with a reduction in the slit width. Equation 10 suggests that the estimation of T_c depends on the difference between coexisting liquid and vapor densities. Higher differences in coexisting densities will result in comparatively higher T_c values. For example, at a reduced temperature of 0.90, the average vapor density decreases by 60% and the liquid density increases by 3.5%, as the slit width is decreased from 15 to 10 Å. On the other hand, the average vapor density decreases by 33% and the liquid density decreases by 12.5% as the slit width decreases from 10 to 9 Å. This remarkable change in coexisting densities is reflected in a sudden relative decrease in the T_c value, with a change in the slit width from 10 to 9 Å. This behavior is also reflected in local *z*-density profiles, as shown in Figure 5a,b, of coexisting vapor and liquid phases of methane in graphite slit pores at these three different slit widths, namely, 9, 10, and 15 Å at a fixed reduced temperature of 0.90. This transition in the slope for different linear regimes for smaller slit widths is indicative of the fact that, in the case of a confinement decrease, the critical temperature does not obey a single linear dependency throughout the range of pore widths. This was also observed recently for a square-well fluid in a hard slit pore.[72]

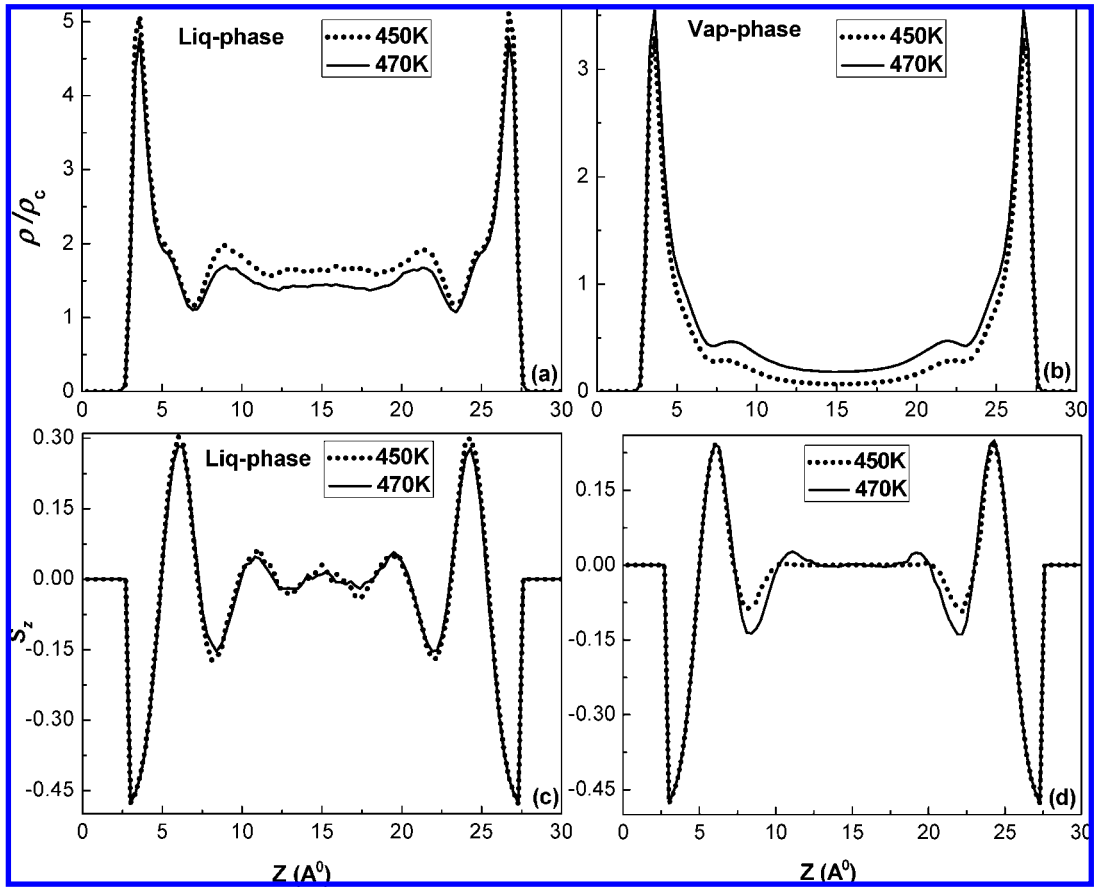

Figure 8. Temperature dependence on the density and orientational profiles of *n*-octane in a mica slit pore for a 30 Å slit width. Plots a and b are saturated liquid and vapor density profiles, respectively, and the corresponding orientation profiles are in given in parts c and d, respectively.

Parts a and b of Figure 6 present corresponding state plots of coexistence envelopes of *n*-butane and *n*-octane in terms of reduced temperature (T/T_c) and density (ρ/ρ_c) for pores with two different slit widths, 40 and 8 Å. Figure 6a shows that, at larger slit width, the coexistence density of the vapor phase in a mica slit pore is more than that in a graphite slit pore, whereas the reverse is the case for the liquid-phase density. However, in a smaller slit-width pore, for example, 8 Å, surface characteristics appear to be noninfluential, as seen in Figure 6b, which shows an indistinguishable behavior of coexistence densities for fluids in graphite and mica pores at two to three molecular diameter slit pores. To gain insight into this behavior, local density and orientational profiles are being studied. Parts a and b of Figure 7 present *z*-density profiles and corresponding orientation profiles of *n*-octane in a 30 Å slit width and at a reduced temperature of 0.93. Figure 7a shows that, in spite of having greater density in the first layer of the liquid-phase profile, which is attributed to the stronger attractive nature of mica as compared to the graphite surface, the overall average liquid density in a mica slit pore is less than that in a graphite slit pore. In contrast, the average density in the vapor phase in a mica pore is more than that in a graphite pore. Similar behavior is observed for other alkanes in higher slit-width pores. A comparison of the orientation profiles of *n*-octane in Figure 7b shows that the molecules in each layer are ordered and lie parallel to the walls ($S_z < 0$). As the distance from the wall increases, the orientation order fluctuates and eventually terminates at zero, indicative of the random nature of the system. We have studied the temperature dependence of the density and corresponding orientation profiles of liquid and vapor phases of a typical case of *n*-alkane (*n*-octane) in a mica slit pore, as shown in Figure 8. Parts a and b of Figure 8 indicate that, with an increase in the temperature, the density of the liquid phase in each layer decreases, whereas the density of the vapor phase increases, as expected. This is also evident from the phase coexistence plots of Figures 2 and 6. On the other hand, the orientation of the molecules in the liquid and vapor phases does not change appreciably with a change in the temperature, especially near the slit surfaces, as shown in Figure 8c,d. This is in agreement with the experimental evidence with long-chain *n*-alkanes in the slit-pore confinement.[73] The experimental evidence of ref 73 along with our study indicates that a change in the temperature has insignificant influence on the orientation of the molecules near the surface.

The vapor-pressure data of a pure substance are fundamentally important for phase equilibrium calculations and engineering applications, such as distillation, evaporation, and two-phase reactors. We have investigated the effect of the extent of confinement in two different types of slit pores on the saturation vapor pressure for a range of temperatures. Parts a and b of Figure 9 show comparisons of the saturation vapor pressure in confinement with respect to bulk, in a corresponding state plot. Saturation vapor pressures under either type of confinement (graphite and mica) show positive and negative deviation with respect to the bulk value at a give reduced temperature. The saturation vapor pressure at larger slit width is more than that of bulk at a given reduced temperature; for *n*-octane, this value is approximately 20 Å in mica and graphite. A subsequent decrease in the slit width (as seen for 10 and 8 Å) reduces the reduced vapor pressure, which is substantially smaller than the corresponding bulk value. A deviation of the reduced vapor pressure from the corresponding bulk value is seen as larger

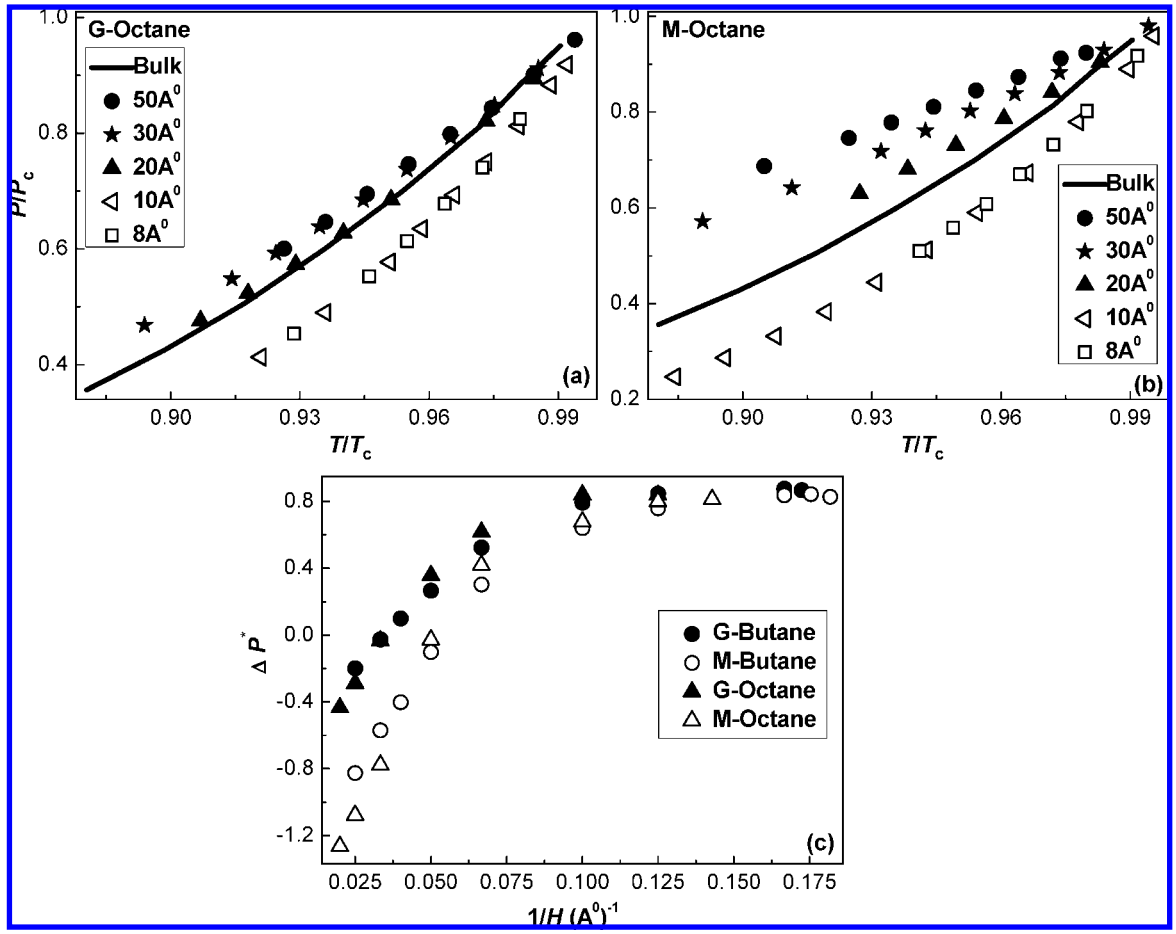

Figure 9. Variation of reduced saturation vapor pressures vs reduced temperature of the bulk and confined *n*-octane in (a) graphite and (b) mica slit pores of varying slit widths. Solid lines represent bulk values; filled and open symbols show positive and negative deviations, respectively. Part c shows the shift in the critical pressure ΔP^* of butane and octane with the inverse of the slit width (H) in graphite (G) and mica (M) slit pores.

for a mica pore because of its stronger attraction. Chen et al.[74] earlier predicted that the nanocapillary pressure of *n*-hexadecane in terms of $\ln(P/P_s)$ vs $1/r$ oscillates when the capillary size, r, approaches a few molecular diameter, which suggests that the behavior of fluids in a nanosize capillary deviates from that of Kelvin's equation. In this work, specific calculations to check the behavior of Kelvin's equation in small pores have not been performed; however, a certain indication of the deviation from Kelvin's equation is probably reflected in our saturation vapor pressures (pressure component parallel to the slit surfaces and perpendicular to the vapor−liquid interface), under confinement, as shown in Figure 9a,b. Nevertheless, a more rigorous study is required to test the correctness of Kelvin's equation and a modified version of it[74] for *n*-alkane in nanocapillaries, which is out of the scope of the current work and is reserved for a future study.

We have also evaluated vapor−liquid critical pressures under various confinement using eq 12, in the same way as was reported for bulk *n*-alkanes[69] and confined square-well fluids[62] in earlier investigations. Equation 12 is used as a fitting tool to calculate the critical pressure once the critical temperature is obtained. Such usage of eq 12 is based on the observation that the logarithm of the saturation pressure under confinement, $\ln(P)$, scales linearly with $1/T$, in a way similar to that for the bulk vapor pressure.[69] In Figure 9c, we have shown the shift in the critical pressure, $\Delta P^* = (P_{cb} - P_{cp})/P_{cb}$, where P_{cb} is the bulk critical pressure and P_{cp} is the confined critical pressure, with the inverse of the slit width. The behavior seen for the critical pressure shift is completely in contrast with the non-monotonic behavior seen for the critical temperature and density. Figure 9c also reflects that the nature of the surface is more dominant on the critical pressure, particularly at larger slit widths, which is not seen for the critical temperature. Such an effect diminishes and disappears as the slit width is reduced toward the two-dimensional value.

One of the advantageous aspects of the GC-TMMC method is that it can be used in conjunction with the finite-size-scaling (FSS) technique of Binder[57] to evaluate surface tension values. The effectiveness of this technique over other methods is demonstrated by Singh and Kofke.[60] This technique also benefits from the ease with which calculations can be performed using multiple processors. The combined GC-TMMC + FSS method has been used to determine surface tension values for Lennard-Jones,[51] square-well,[60] model associating fluids[61] and chain molecules.[69] In this work, we have investigated the effect of the surface characteristics and the extent of confinement on the vapor−liquid surface tension of *n*-alkanes. Our investigation indicates that the bulk vapor−liquid surface tension of *n*-alkanes decreases under confinement of graphite (G) and mica (M) slit pores. This reduction of the surface tension is attributed to the reduction in the vapor−liquid surface free energy due to confinement. Parts a−e of Figure 10 present a comparison of the vapor−liquid surface tension of bulk *n*-alkane evaluated with the truncated exp-6 potential with $r_c = 15$ Å and the same under different slit-pore confinement. The surface tension diminishes with a decrease in the slit width because for a given temperature

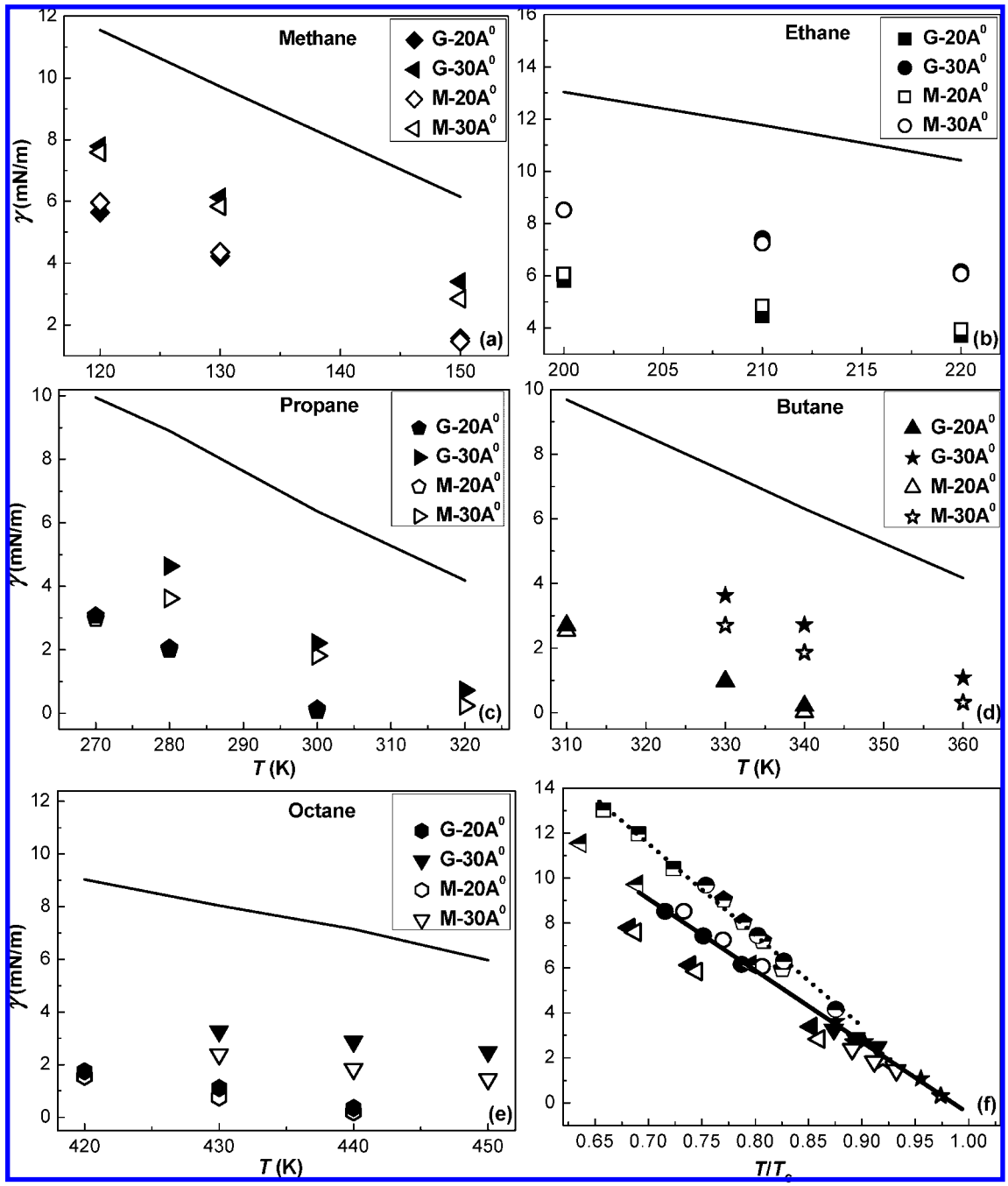

Figure 10. Vapor−liquid surface tensions of bulk and confined (a) methane, (b) ethane, (c) propane, (d) butane, and (e) octane in graphite (G) and mica (M) pores for two slit widths, 20 and 30 Å. Solid lines represent the bulk surface tension value (data points are the same as those reported in Figure 1c, with open symbols) obtained with r_c = 15 Å without LRC. In part f, the surface tensions of bulk and confined methane, ethane, butane, and octane are shown versus the reduced temperature (T/T_c). Surface tensions of confined *n*-alkanes are shown only with 30 Å slit width of graphite and mica surfaces, with dotted and solid lines representing fits to the data of bulk and confined *n*-alkanes, respectively. Filled and open symbols represent the surface tension values of fluids in graphite and mica slit pores, respectively, and have the same meaning as those in parts a−e. Half-filled symbols (half-left triangle for methane, half-square for ethane, half-circle for butane, and half-pentagon for octane), in part f, represent bulk phase simulated data points of *n*-alkanes. The error bars are smaller than the symbol size.

the free energy difference with respect to the interface decreases with a reduction in the slit width. However, for a constant slit width, the interfacial free energy decreases with an increase of the temperature; hence, the vapor−liquid surface tension decreases with an increase of the temperature as expected. We also observed that, in general, at the same absolute temperature, for a 30 Å slit width, the reduction in the vapor−liquid surface tension from the bulk is more for the mica (M) slit pore than for the graphite (G) slit pore, especially for comparatively longer chain molecules (C_3 or higher). Conversely, this trend is not observed for the smaller pore width of 20 Å, which perhaps is the signature of insensitiveness of the thermophysical properties toward the surface characteristic at such a scale of confinement. This is also reflected from the corresponding state plot of orthobaric densities, as seen in Figure 6b. Figure 10f presents the vapor−liquid surface tension of bulk and confined *n*-alkanes as a function of reduced temperatures (T/T_c). Interestingly, the surface tension values of all typical bulk *n*-alkanes, except for methane, studied in this work fall reasonably around one linear curve, as shown by the dotted line for the range of studied

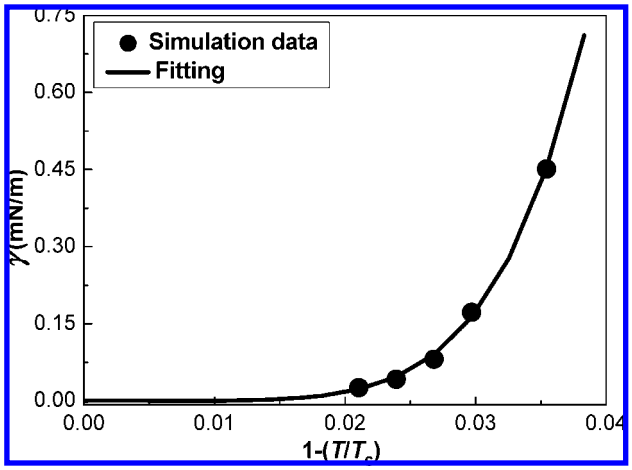

Figure 11. Vapor−liquid surface tension, γ, of *n*-butane in a mica slit pore vs $(1 - T)/T_c$. Symbols represent the simulation data obtained with the FSS technique, and the solid line is a fit of the data.

temperatures. Surprisingly, the behavior remains the same for the confined fluid; however, the slope of the master curve for the confined fluid, as shown by the solid line, is less than that of the bulk fluid. Figure 10f contains surface tension data for *n*-alkanes in a slit pore of 30 Å slit width. Corresponding data in a 20 Å slit width (data not shown for the sake of clarity) fall also on the same linear curve, except for methane. The probable reason for deviation of methane from the master curve is its spherical nature, as compared to the other chain molecules. It is apparent from Figure 10f that bulk phase surface tension values and corresponding confined values are different at the same reduced temperature, specifically at lower temperatures. In particular, confinement diminishes the surface tension value at a given reduced temperature. As the temperature increases, such that $T/T_c > 0.9$, both bulk and confined surface tension values appear to collapse on each other, which indicates the insignificant role of confinement and surface characteristics on the surface tension at high temperature.

It is known that critical property calculation from the rectilinear approach is an approximate technique compared to the more rigorous FSS technique.[75] Hence, we have verified the correctness of the critical temperature, estimated in this work, with the value extrapolated from the surface tension values at higher temperatures. We have evaluated some of the vapor−liquid surface tension values using the GC-TMMC + FSS technique, at some higher temperatures, namely, 335, 337, 338, 339, and 340 K for a typical case of alkane, *n*-butane. Surface tension, γ, data calculated at the above temperatures are used for extrapolation to obtain the critical temperature as γ approaches zero. Figure 11 presents the simulation data and the fitted curve. The critical temperature obtained through the above method is extremely close to our calculation based on the rectilinear diameter approach. For example, in the case of butane in a mica slit pore of 20 Å slit width, the T_c value estimated from the rectilinear approach is 347.31 K and the extrapolated surface tension value at 347.31 K is around 2.24×10^{-24}, which is practically zero. This suggests that the technique employed for calculation of the critical temperature in this work gives reasonably accurate results.

4. Conclusions

The configurational-bias Monte Carlo technique combined with the original GC-TMMC formalism produces an efficient and self-adaptive method for evaluating the thermophysical properties of alkanes in nanopores. Our investigations indicate that the surface characteristics and the extent of confinement affect dramatically various properties of *n*-alkanes. The critical temperature decreases continuously up to a certain minimum slit width, and then it becomes constant as the system approaches the two-dimensional regime. We observed that a shift in the critical temperature with respect to the bulk value follows more than two linear regimes as a function of the inverse slit width from nearly three-dimensional to two-dimensional geometry. The critical density, on the other hand, fluctuates with a decrease in the slit width. On the other hand, a shift in the critical pressure monotonically increases with a decrease in the slit width and approaches to a constant value at a smaller pore. Corresponding state plots suggest that the deviation of the saturation vapor pressure from the bulk saturation pressure, for a range of temperatures, under confinement is positive for large pores and negative for smaller pores. As the temperature approaches T_c, this deviation slowly disappears. The corresponding state plot reveals that at higher slit width vapor−liquid coexistence properties are sensitive to the nature of the interacting surfaces. On the other hand, these properties are seemingly insensitive to the surface characteristics at the smaller pore width. Liquid−vapor surface tension values for *n*-alkanes in graphite and mica pores are studied, for the first time, and found to be suppressed by many fold under confinement.

Acknowledgment. This work was supported by the Department of Science and Technology, Government of India (Grants SR/S3/CE10/2006 and IR/S3/EU/005/2007). We acknowledge further computational support from the Computer Center, Indian Institute of Technology Kanpur.

References and Notes

(1) Gelb, L. D.; Gubbins, K. E.; Radhakrishnan, R.; Sliwinska-Bartkowiak, M. *Rep. Prog. Phys.* **1999**, *62*, 1573.
(2) Jackson, C. L.; McKenn, G. B. *J. Chem. Phys.* **1990**, *93*, 9002.
(3) Lee, S. C.; Cheng, H. S. *Tribol. Trans.* **1991**, *113*, 327.
(4) Gupta, S. A.; Cochran, H. D.; Cummings, P. T. *J. Chem. Phys.* **1997**, *107*, 10327.
(5) Israelachvili, J. N. *Intermolecular and Surface Forces*; Academic: New York, 2003.
(6) Baljon, A. R. C.; Robbins, M. O. *Mater. Res. Bull.* **1997**, *22*, 22.
(7) Matranga, K. R.; Myers, A. L.; Glandt, E. D. *Chem. Eng. Sci.* **1992**, *47*, 1569.
(8) Bhatia, S. *Langmuir* **1998**, *14*, 6231.
(9) Altwasser, S.; Welker, C.; Traa, Y.; Weitkamp, J. *Microporous Mesoporous Mater.* **2005**, *83*, 345.
(10) Maciver, D. S.; Emmett, P. H.; Frank, H. S. *J. Phys. Chem.* **1958**, *62*, 935.
(11) Gregg, S. J.; Sing, K. S. W. *Adsorption, Surface Area, and Porosity*, 2nd ed.; Academic: New York, 1982.
(12) Liapis, A. J., Ed. *Fundamentals of Adsorption*; Engineering Foundation: New York, 1987.
(13) Rouquerol, F.; Rouquerol, J.; Sing, K. S. W. *Adsorption by Powders and Porous Solids: Principles, Methodology, and Applications*; Academic: San Diego, 1999.
(14) Rowlinson, J. S.; Widom, B. *Molecular Theory of Capillarity*; Oxford University Press: London, 1982.
(15) Croxton, C. A., Ed. *Fluid Interfacial Phenomena*; Wiley: New York, 1985.
(16) Charvolin, J., Joanny, J.-F., Zinn-Justin, J., Eds. *Liquids at Interfaces*; North-Holland: Amsterdam, The Netherlands, 1990.
(17) Henderson, D., Ed. *Fundamentals of Inhomogeneous Fluids*; Dekker: New York, 1992.
(18) Binder, K.; Landau, D.; Müller, M. *J. Stat. Phys.* **2003**, *110*, 1411.
(19) Fuchs, A. H.; Cheetham, A. K. *J. Phys. Chem. B* **2001**, *105*, 7375.
(20) Smit, B.; Siepmann, J. I. *Science* **1994**, *264*, 1118.
(21) Fox, J. P.; Roy, V.; Bates, S. P. *Microporous Mesoporous Mater.* **2004**, *69*, 9.
(22) Gupta, A.; Clark, L. A.; Snurr, R. Q. *Langmuir* **2000**, *16*, 3910.
(23) Chempath, S.; Denayer, J. F. M.; De Meyer, K. M. A.; Baron, G. V.; Snurr, R. Q. *Langmuir* **2004**, *20*, 150.

(24) Jiang, J. W.; Sandler, S. I.; Schenk, M.; Smit, B. *Phys. Rev. B* **2005**, *72*, 045447.
(25) Jiang, J. W.; Sandler, S. I. *Fluid Phase Equilib.* **2005**, *228*, 189.
(26) Duren, T.; Sarkisov, L.; Yaghi, O. M.; Snurr, R. Q. *Langmuir* **2004**, *20*, 2683.
(27) Frost, H.; Duren, T.; Snurr, R. Q. *J. Phys. Chem. B* **2006**, *110*, 9565.
(28) Zhang, F. *J. Chem. Phys.* **1999**, *111*, 9082.
(29) Do, D. D.; Do, H. D. *J. Phys. Chem. B* **2005**, *109*, 19288.
(30) Kowalczyk, P.; Tanaka, H.; Kaneko, K.; Terzyk, A. P.; Do, D. D. *Langmuir* **2005**, *21*, 5639.
(31) Vishnyakov, A.; Piotrovskaya, E. M.; Brodskaya, E. N. *Langmuir* **1996**, *12*, 3643.
(32) Klochko, V. A.; Brodskaya, E. N.; Piotrovskaya, E. M. *Langmuir* **1999**, *15*, 545.
(33) Calleja, G.; Coto, B.; Pinar, A.; Morales-Cas, A. M. *Adsorption* **2006**, *12*, 45.
(34) Do, D. D.; Do, H. D. *Chem. Eng. Sci.* **2005**, *60*, 1977.
(35) Severson, B. L.; Snurr, R. Q. *J. Chem. Phys.* **2007**, *126*, 134708.
(36) Balasundaram, R.; Jiang, S. Y.; Belak, J. *Chem. Eng. J.* **1999**, *74*, 117.
(37) Wang, J. C.; Fichthorn, K. A. *Colloids Surf. A* **2002**, *206*, 267.
(38) Cui, S. T.; Gupta, S. A.; Cummings, P. T.; Cochran, H. D. *J. Chem. Phys.* **1996**, *105*, 1214.
(39) Cui, S. T.; Cummings, P. T.; Cochran, H. D.; Moore, J. D.; Gupta, S. A. *Int. J. Thermophys.* **1998**, *19*, 449.
(40) Martini, A.; Liu, Y.; Snurr, R. Q.; Wang, Q. J. *Tribol. Lett.* **2006**, *21*, 217.
(41) Ryckaert, J. P.; Bellemans, A. *Chem. Phys. Lett.* **1975**, *30*, 123.
(42) Errington, J. R.; Panagiotopoulos, A. Z. *J. Phys. Chem. B* **1999**, *103*, 6314.
(43) Van der Ploeg, P.; Berendsen, H. J. C. *J. Chem. Phys.* **1982**, *76*, 3271.
(44) Smit, B.; Karaborni, S.; Siepmann, J. I. *J. Chem. Phys.* **1995**, *102*, 2126.
(45) Steele, W. A. *Surf. Sci.* **1972**, *36*, 317.
(46) Porcheron, F.; Rousseau, B.; Fuchs, A. H.; Schoen, M. *Phys. Chem. Chem. Phys.* **1999**, *1*, 4083.
(47) Siepmann, J. I.; Frenkel, D. *Mol. Phys.* **1992**, *75*, 59.
(48) De Pablo, J. J.; Laso, M.; Suter, U. W. *J. Chem. Phys.* **1992**, *96*, 2395.
(49) Rosenbluth, M. N.; Rosenbluth, A. W. *J. Chem. Phys.* **1956**, *23*, 356.
(50) Errington, J. R. *Phys. Rev. E* **2003**, *67*, 012102.
(51) Errington, J. R. *J. Chem. Phys.* **2003**, *118*, 9915.
(52) Berg, B. A.; Nneuhaus, T. *Phys. Rev. Lett.* **1992**, *61*, 9.
(53) Fitzgerald, M.; Picard, R. R.; Silver, R. N. *Europhys. Lett.* **1999**, *46*, 282.
(54) Fitzgerald, M.; Picard, R. R.; Silver, R. N. *J. Stat. Phys.* **2000**, *98*, 321.
(55) Ferrenberg, A. M.; Swendsen, R. H. *Phys. Rev. Lett.* **1988**, *61*, 2635.
(56) Goujon, F. M.; Boutin, A.; Fuchs, A. H. *J. Chem. Phys.* **2002**, *116*, 8106.
(57) Binder, K. *Phys. Rev. A* **1982**, *25*, 1699.
(58) Potoff, J. J.; Panagiotopoulos, A. Z. *J. Chem. Phys.* **2000**, *112*, 6411.
(59) Singh, J. K.; Kofke, D. A.; Errington, J. R. *J. Chem. Phys.* **2003**, *119*, 3405.
(60) Singh, J. K.; Kofke, D. A. *Mol. Simul.* **2004**, *30*, 343.
(61) Singh, J. K.; Kofke, D. A. *J. Chem. Phys.* **2004**, *121*, 9574.
(62) Singh, J. K.; Kwak, S. K. *J. Chem. Phys.* **2007**, *126*, 24702.
(63) Rowlinson, J. S.; Swinton, F. L. *Liquids and Liquid Mixtures*, 3rd ed.; Butterworth: London, 1982.
(64) Rowlinson, J. S.; Widom. B. *Molecular Theory of Capillarity*; Clarendon: Oxford, U.K., 1982.
(65) Errington, J. R. *Langmuir* **2004**, *20*, 3798.
(66) Baidakov, V. G.; Chernykh, G. G.; Protsenko, S. P. *Chem. Phys. Lett.* **2000**, *321*, 315.
(67) Goujon, F.; Malfreyt, P.; Boutin, A.; Fuchs, A. H. *J. Chem. Phys.* **2002**, *116*, 8106.
(68) NIST Chemistry Web Book. http://webbook.nist.gov/chemistry/fluid.
(69) Singh, J. K.; Errington, J. R. *J. Phys. Chem. B* **2006**, *110*, 1369.
(70) Bruno, E.; Marini Bettolo Marconi, U.; Evans, R. *Physica A* **1987**, *141*, 187.
(71) Vishnyakov, A.; Piotrovskaya, E. M.; Brodskaya, E. N.; Votyakov, E. V.; Tovbin, Yu. K. *Langmuir* **2001**, *17*, 4451.
(72) Subimal, J.; Singh, J. K.; Kwak, S. K. *J. Chem. Phys.* **2008**, submitted for publication.
(73) Maeda, N.; Kohonen, M. M. *J. Phys. Chem. B* **2001**, *105*, 5906.
(74) Chen, Y.; Wetzel, T.; Aranovich, G. L.; Donohue, M. D. *J. Colloid Interface Sci.* **2006**, *300*, 45.
(75) Wilding, N. B. *Phys. Rev. E* **1995**, *52*, 602.

JP8073915